Editors' Suggestion

Deterministic Remote Entanglement of Superconducting Circuits through Microwave Two-Photon Transitions

P. Campagne-Ibarcq,* E. Zalys-Geller, A. Narla, S. Shankar, P. Reinhold, L. Burkhart, C. Axline, W. Pfaff, L. Frunzio, R. J. Schoelkopf, and M. H. Devoret†
Department of Applied Physics, Yale University, New Haven, Connecticut 06511, USA

(Received 15 December 2017; published 16 May 2018)

Large-scale quantum information processing networks will most probably require the entanglement of distant systems that do not interact directly. This can be done by performing entangling gates between standing information carriers, used as memories or local computational resources, and flying ones, acting as quantum buses. We report the deterministic entanglement of two remote transmon qubits by Raman stimulated emission and absorption of a traveling photon wave packet. We achieve a Bell state fidelity of 73%, well explained by losses in the transmission line and decoherence of each qubit.

DOI: 10.1103/PhysRevLett.120.200501

Introduction.—Entanglement, which Schrödinger described as "*the* characteristic trait of quantum mechanics" [1], is instrumental for quantum information science applications such as quantum cryptography and all the known pure-state quantum algorithms [2]. Two distant systems Alice and Bob can be entangled if they interact locally with a third traveling system acting as a mediator. Since they can travel over long distances, photons are natural candidates for this role [3].

Remote entanglement was first demonstrated between two atomic clouds [4] traversed by a light beam measuring nondestructively a joint property. The difficulty of this scheme is to render the extracted information from the two systems indistinguishable. Superconducting circuit implementations [5,6] also face this issue. Another protocol, widely used in trapped ions [7], solid-state spin qubits [8], quantum dots [9], and superconducting circuits [10], relies on the simultaneous emission of photons by both Alice and Bob, either through fluorescence or stimulated Raman emission. Entanglement is then heralded by detection of one of these photons, whose origin is erased by recombining them on a beam splitter. This scheme is robust, in particular against photon losses, as long as the photons are indistinguishable to the detector. It should be possible to entangle in this way two arbitrary nodes of a network for modular quantum computing [11–13]. But can we build an even simpler remote entangler, which would not require a which-path eraser and detector?

As depicted in Fig. 1(a), a minimal protocol consists of entangling Alice with a propagating electromagnetic field—for instance, by concurrently exciting the standing system and a photon in this field—whose state is then *swapped* to Bob. Entanglement of atomic clouds using this method was reported in Ref. [14], albeit with very low success probability. On the other hand, *deterministic* generation of entanglement requires an efficient absorption by one node of the field emitted by the other, which is also desirable to propagate information through a network.

Efficient absorption by the receiving node requires shaping the "pitched" wave packet by controlling the emission rate in time at the emitting node [15,16]. In circuit QED, many experiments [17–21] have focused on pitching a rising exponential wave packet, which can be easily absorbed [22–25] by the receiver. Another approach [15,26] consists of modulating both the emitter and receiver couplings to the transmission channel in time to pitch and catch a time-symmetric wave packet. While efforts were made in that direction [27–29], the full protocol has not been demonstrated so far [30].

In this Letter, we report deterministic entanglement generation between two distant transmon superconducting qubits using such a scheme. We employed microwave pumps to concurrently and coherently excite a transmon and a photon in a buffer resonator [10,20]. The photon leaks out in a transmission line, and after traveling along $\sim$1 m cable and through microwave components is captured by a second transmon qubit with a similar scheme. The entanglement purity is limited by photon losses in the line, which could be corrected for by purification [33,34], and intrinsic decoherence of each qubit, which could also be improved.

Driving a two-photon transition.—The experimental setup is schematically depicted in Fig. 1(b). Two superconducting transmon qubits [35], Alice and Bob, are embedded in two indium-plated copper cavities, anchored to the base stage of a dilution refrigerator (see Refs. [10,36] for device fabrication and setup details). The photon damping rate $\kappa = 2\pi \times 1$ MHz for the lowest energy mode of each cavity is set by relaxation through a well-coupled port into a common microwave transmission line, which dominates over both the internal losses and relaxation through a second port. This last port is used to apply resonant microwave drives

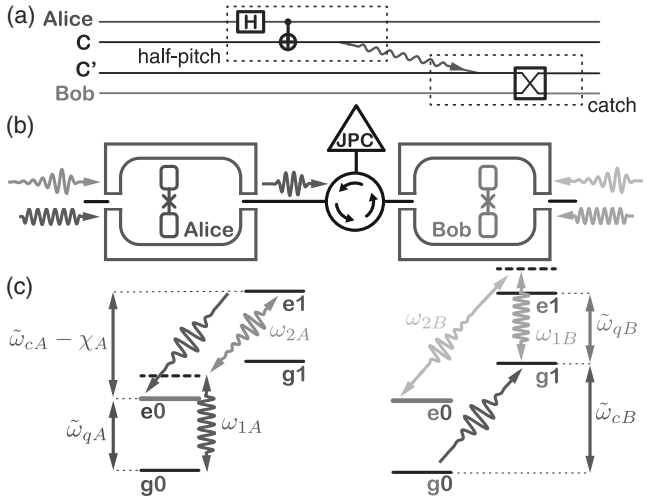

FIG. 1. (a) Minimal logical circuit for remote entanglement. Alice is entangled with the ancillary system C by a Hadamard and a CNOT gate. The information propagates to C′ (green wave) where it is *swapped* to Bob. (b) Setup schematics and (c) energy level diagram. Two transmon qubits Alice (in dark blue, dressed frequency $\tilde{\omega}_{qA}$, see text for details) and Bob (in red, dressed frequency $\tilde{\omega}_{qB}$) are dispersively coupled to two resonant cavities (in green, dispersive couplings $\chi_{A,B}$). The cavities' lowest energy modes are frequency matched ($\tilde{\omega}_{cA}-\chi_A \simeq \tilde{\omega}_{cB}$) and are strongly coupled to a directional transmission line routing photons from Alice to Bob. By simultaneously driving Alice (Bob) with the detuned purple microwave at ω_{1A} (orange, at ω_{1B}) and her cavity with the detuned light blue microwave at ω_{2A} (light pink, at ω_{2B}), we drive a Raman-type two-photon transition. For Alice, we choose $\omega_{1A}+\omega_{2A}=\tilde{\omega}_{qA}+\tilde{\omega}_{cA}-\chi_A$ to resonantly drive $|g0\rangle \leftrightarrow |e1\rangle$ (see (c), left-hand diagram). A photon can eventually be emitted in the line (green wave). The wave packet is shaped by modulating the pump amplitude. This photon is absorbed by Bob by driving $|g1\rangle \leftrightarrow |e0\rangle$ with $\omega_{2B}-\omega_{1B}=\tilde{\omega}_{cB}-\tilde{\omega}_{qB}$ (right-hand diagram). After a full photon pitch and catch, the system is in $|e0\rangle_A|e0\rangle_B$ (in magenta). After a "half" pitch, the qubits are entangled. The output field from Bob is directed to a high efficiency detection line (JPC) used for calibration and qubit measurements (see text).

to perform control operations on a single mode, such as qubit rotations at $\omega_{qA,qB}/2\pi \sim 5\,\mathrm{GHz}$, or cavity displacements at $\omega_{cA,cB}/2\pi \sim 7.5$ GHz. Interestingly, we can also directly drive common two-excitation transitions of these modes such as $|g0\rangle \leftrightarrow |e1\rangle$ or $|g1\rangle \leftrightarrow |e0\rangle$ [40]. Here, $|0\rangle$ and $|1\rangle$ designate Fock states of the cavity and $|g\rangle$ and $|e\rangle$ the ground and first excited states of the qubit. This is done by simultaneously applying a sideband pump at $\omega_{1A,1B}$ detuned from the qubit frequency by $\Delta/2\pi = 100$ MHz (purple and orange waves on Fig. 1) and another at $\omega_{2A,2B}$ detuned from the cavity frequency by $\pm\Delta$ (light blue and pink waves).

Let us consider separately each system Alice *or* Bob. One can show [36,41,42] that in a displaced frame and using a rotating wave approximation the system Hamiltonian in the presence of pumps at ω_1 and ω_2 reads

$$\begin{aligned}\frac{H}{\hbar} &= \tilde{\omega}_q(t)q^\dagger q + \tilde{\omega}_c(t)c^\dagger c - \frac{\alpha}{2}(q^\dagger q)^2 - \chi q^\dagger q c^\dagger c \\ &+ e^{-i(\omega_1+\omega_2)t} g_s(t) q^\dagger c^\dagger + \text{H.c.} \\ &+ e^{-i(\omega_1-\omega_2)t} g_c(t) q^\dagger c + \text{H.c.}, \end{aligned} \tag{1}$$

where c and q are the annihilation operators for the cavity and qubit modes, α is the anharmonicity of the transmon mode, χ the dispersive shift [43], and $\tilde{\omega}_q(t)$ and $\tilde{\omega}_c(t)$ are the Stark shifted frequencies of the transmon and cavity modes in the presence of the pumps. These dressed frequencies and the *squeezing* and *conversion* strengths $g_s(t)$ and $g_c(t)$ are slow varying compared to Δ and read

$$\tilde{\omega}_q = \omega_q - \chi|\xi_2|^2 - 2\alpha|\xi_1|^2, \tag{2a}$$

$$\tilde{\omega}_c = \omega_c - \chi|\xi_1|^2, \tag{2b}$$

$$g_s = \chi\xi_1\xi_2, \tag{2c}$$

$$g_c = \chi\xi_1\xi_2^*. \tag{2d}$$

Here, ω_q and ω_c are the frequencies in the absence of the pumps. ξ_1 and ξ_2 are the effective pump amplitudes—which correspond to the frame displacements used to get to Eq. (1)—and are proportional to the amplitude of the pump tones. Note that since the cavity mode is only weakly anharmonic, we have neglected a frequency shift of the cavity mode proportional to $|\xi_2|^2$ [36].

The conversion or squeezing process (red or blue sideband) can be selected by setting either

$$\tilde{\omega}_q + \tilde{\omega}_c - \chi = \omega_1 + \omega_2 \rightarrow |g0\rangle \leftrightarrow |e1\rangle, \tag{3a}$$

$$\tilde{\omega}_q - \tilde{\omega}_c = \omega_1 - \omega_2 \rightarrow |g1\rangle \leftrightarrow |e0\rangle, \tag{3b}$$

in driving the two-photon transition. The resonance condition Eq. (3a) is used for Alice. As shown by the energy-level diagram of Fig. 1, this pumping, combined with the cavity dissipation, eventually brings the system to the state $|e0\rangle$ (highlighted in magenta). If the qubit is initially in $|g\rangle$, a photon is emitted in the line (green wave). Conversely, the resonance condition Eq. (3b) is used for Bob, and if the qubit is initially in $|g\rangle$, it can absorb the incoming photon and excite to $|e\rangle$ (level highlighted in magenta), provided that the photon is resonant with the cavity frequency. This is made possible by designing the two cavities so that their transitions nearly match $[(\omega_{cA}-\chi-\omega_{cB})/2\pi = 600$ kHz], and by modulating the amplitude and frequency of the pumps in time [see Fig. 3(a)], in order to shape the pitched wave packet and to catch it efficiently. Accurate control of the drive strengths while matching the resonance conditions Eq. (3) is the main difficulty of this experiment.

First, we must determine the unknown scaling factor linking the amplitude of the applied pumps to the effective

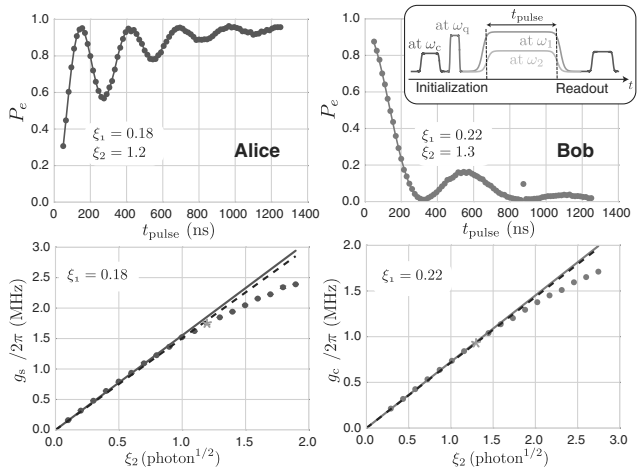

FIG. 2. Top: Rabi oscillations when driving a two-photon transition for a varying duration $t_{\rm pulse}$ are recorded in the qubit excited state populations (dots). Alice is initialized in $|g\rangle$ and Bob in $|e\rangle$. The pump amplitude values ξ_1 and ξ_2 are calibrated through Stark-shift measurements (see text and Ref. [36]). As for all population measurements presented in this Letter, statistical error bars are smaller than the dot size. Lines are fits for the two-photon drive strengths g_s and g_c. Inset: Pulse sequence schematics. Pump pulse edges are smoothed to 128 ns and the pump 1 pulse is 100 ns longer for accurate control of the drive ramp-up and -down. Bottom: The extracted drive strengths are plotted when varying ξ_2 (dots, the green stars are from the top panel fits). For each point, the cavity pump frequency is tuned to match the resonance condition Eq. (3). Lines are linear fits of the nonsaturated regions and their slopes are used as a calibration for the release and capture of a shaped photon. Dashed black lines are the drive strengths $|g_{c,s}| = \chi|\xi_1\xi_2|$ predicted from Stark shift calibration of $\xi_{1,2}$ [36].

amplitudes $\xi_{1A,2A,1B,2B}$. This is done by measuring the shift of the qubit transition peaks in the presence of the pumps and using Eq. (2a), or any other quantity predicted by Eq. (2). Such spectroscopic measurements are presented in Ref. [36]. While the Stark shifts display a characteristic linear dependence in the pump powers, some of the predictions from Eq. (2b) do not agree quantitatively (a detailed analysis is presented in Ref. [36]). In practice, we use an empirical approach. The amplitude of the two-photon drives being determined by the product of the pump amplitudes, we set ξ_1 and ω_1 at a constant value. The cavity frequency is then fixed [see Eq. (2b)], and so is the frequency of the released photon. To vary g_s or g_c, we only vary ξ_2 and change accordingly the frequency ω_2 to fulfill the resonance condition Eq. (3).

Following this protocol, we record Rabi oscillations of these two-photon transitions, presented in Fig. 2. The qubits are first initialized in $|g\rangle$ (Alice) or $|e\rangle$ (Bob) by single-shot dispersive measurement using a near quantum limited Josephson parametric converter [44,45] and fast feedback control [46,47]. We then drive the two-photon transition for a varying time $t_{\rm pulse}$. For Alice, we record an oscillation in the excited state population decaying to 1 at a rate κ, as $|e\rangle$ is a dark state in the presence of cavity dissipation (see Fig. 1). The edges of the pulses are smoothed as depicted in the top right inset so that the oscillation does not start at $P_e = 0$. We can fit this oscillation with g_s as the only free parameter by solving a quantum Langevin equation [36,48] on the qubit and cavity modes. Inversely, for Bob (right-hand panel), the excited state population decays to 0. Note that this feature can be used for efficient cooling of the qubits before the experiment [36,49]. In both cases, we then repeat the measurement when varying ξ_2. The extracted values of g_s and g_c display the expected linear dependence at low pump power (lines are linear fits) and are in good agreement with predictions from Eqs. (2c) and (2d) with the values of ξ_1, ξ_2 and dispersive shifts $\chi_A/2\pi = 8.3$ MHz, $\chi_B/2\pi = 3.3$ MHz extracted from spectroscopic measurements [36] (dashed black lines). This provides an accurate calibration of the drive strengths at low pump amplitude. Saturation for stronger drives is mainly attributed to nonideal behavior of the mixers used to generate the pulses. Our model also neglected some nonlinear effects such as the anharmonicity inherited by the cavity mode [36] and the nonconfining nature of the transmon *cosine* potential. For the actual release and capture presented in the next sections, we use smaller values of $\xi_1 = 0.11$ and $\xi_2 < 1$ (see Ref. [36] for the corresponding Rabi oscillations) as the qubit coherence times were degraded at larger drive amplitude. This unexpected effect may originate from the aforementioned nonidealities, compounded by the small pump detuning Δ—limited by our pulse generation scheme (see Fig. S1 in Ref. [36])—compared to the transmon anharmonicity ($\Delta < \alpha_{A,B} \sim 2\pi \times 200$ MHz).

Excitation transfer.—After calibrating the drive strengths, we turn to the task of generating a photon with Alice and capturing it with Bob. We choose the traveling wave packet to be time symmetric [15], Gaussian shaped for spectral resolution, and with as short a characteristic time $\sigma = 800$ ns as permitted by the aforementioned maximum pump amplitudes. We also scale the wave packet to contain one photon. With these constraints, the values of g_s and g_c required for the transfer are computed using a method adapted from Ref. [26] and described in detail in Ref. [36]. Note that beyond the slowly varying envelopes represented in Fig. 3(a), the pump 2 pulses are modulated at ω_2 and chirped to match the resonance conditions Eq. (2) at all times.

Unlike the ideal case of two perfectly frequency-aligned cavities [15], Alice and Bob's control are not time symmetric of one another. Indeed, to compensate for the small cavity mismatch, we modify Alice's resonance condition Eq. (3a), so that the pitched wave packet does not rotate in Bob's frame. The resulting control g_s is slowly rotating and has a larger amplitude to compensate for this detuning. More generally, frequency mismatch of the order of a cavity linewidth would be tolerable when performing operations

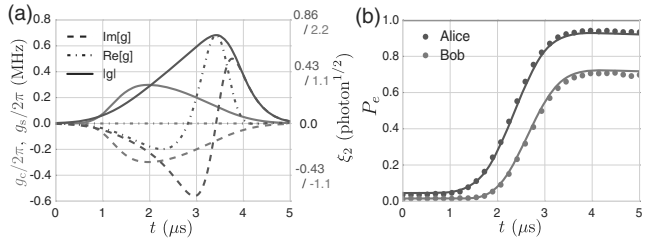

FIG. 3. Release and capture of a shaped photon. (a) Calculated complex amplitude of the two-photon drive strength for Alice (blue) and Bob (red) to transfer a photon in a Gaussian traveling mode centered at Bob's cavity resonance frequency with deviation $\sigma = 800$ ns. These controls are realized by holding ξ_1 constant and varying ξ_2 as represented on the right-hand axis. (b) Excited state populations of Alice and Bob during the transfer (dots), measured by interrupting the transfer control pulses after a duration t and subsequent dispersive readout of the qubits. Lines are predictions from cascaded quantum system simulation including all imperfections.

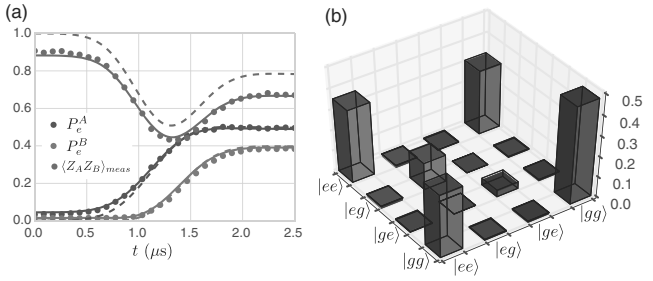

FIG. 4. With Alice and Bob initially in $|g\rangle$, a pump control signal is applied on Alice to release half a photon (see text) while the capture sequence of Fig. 3(a) is played for Bob. (a) Measured excited state populations and correlator (with $Z = 2|e\rangle\langle e| - 1$) when interrupting the control pulses after a duration t and then performing simultaneous dispersive readout on both qubits. Plain lines are simulations including all imperfections. Dashed lines are the same simulations assuming perfect final readouts. (b) Real part of the density matrix of the final entangled state measured by tomography of the two-qubit state (colored bars) and reconstituted by simulation (black contours). Fidelity to the Bell state $(|gg\rangle + |ee\rangle)/\sqrt{2}$ is 73%.

between two nodes of a network, at the expense of using larger drive amplitudes.

The photon transfer is validated by measuring the qubit populations in time [Fig. 3(b)], which reveals a transfer efficiency of 70%, when not correcting for any experimental imperfections. After calibrating those through independent measurements [36], we reproduce the results with 1% accuracy by performing full cascaded quantum system simulations [48] (lines). The dominant error sources are decoherence of the qubits (11% error) and photon loss in the line (15% error) [36]. This last figure is obtained by measurement induced dephasing and confirmed by measuring the fraction of the traveling wave packet power actually absorbed by Bob during the transfer (see Ref. [36]).

Remote entanglement.—We now turn to the task of entangling Alice and Bob. This is done by first having Alice release "half" of a photon and thus getting entangled with the traveling mode in the state $(|g0\rangle + |e1\rangle)/\sqrt{2}$, which corresponds to the Hadamard and CNOT gates in Fig. 1(a). This operation is followed by a SWAP gate between the traveling mode and Bob, which corresponds to the same capture sequence as for the excitation transfer. The controls are determined with the same constraints but scaling the pitched wave packet to contain $1/2$ photon on average. The amplitude of g_s in this case is smaller than for the full release, so that we can use a traveling wave packet with a reduced characteristic time $\sigma = 450$ ns. We plot the measured populations of Alice and Bob during the transfer in Fig. 4(a) (red and blue dots), which agree with the simulation predictions (lines) performed with the same parameters. We also plot the measured correlator $\langle Z_A Z_B \rangle_{\mathrm{meas}}$ (where $Z = 2|e\rangle\langle e| - 1$) between these measurements (green dots). When considering the correlations after correcting for readout errors (dashed lines), we find that at final time the actual occupation of the excited state is $P(|e\rangle_A) = 0.5$ and the actual correlator is $\langle Z_A Z_B \rangle = 2P(|e\rangle_B)$ (within 1%), which implies that Bob is excited *only if* Alice is. In other words, as a photon detector, Bob's false positive probability beyond dispersive readout imperfections is below our detection precision. This property is crucial in nondeterministic entangling schemes, where the catch protocol could be used to perform single microwave photon detection [10,50,51].

Finally, we perform full tomography of the final joint state of Alice and Bob by rotating the qubits to measure all Pauli operators X, Y, and Z and their correlators. After rotating the (X_B, Y_B) basis to compensate for the *a priori* unknown but deterministic differential phase accumulated by control and pump pulses along the input lines, one can directly compute the density matrix following $\rho = \frac{1}{4}\sum_{\alpha,\beta\in\{I,X,Y,Z\}} \langle \alpha_A \beta_B \rangle_{\mathrm{meas}} \alpha_A \otimes \beta_B$. The fidelity to the target Bell state $|\Phi_+\rangle = (|gg\rangle + |ee\rangle)/\sqrt{2}$ is found to be $F = \mathrm{Tr}(\rho|\Phi_+\rangle\langle\Phi_+|) = 73\%$, well above the entanglement threshold $F = 1/2$. Once again, the measured density matrix (color bars in Fig. 4(b); see Ref. [36] for a full representation of the two-qubit state Pauli vector components) is in quantitative agreement with simulation predictions (black transparent bars). The contribution of each experimental imperfection to the infidelity $1 - F$ is detailed in Ref. [36].

In this experiment, we have implemented a simple protocol to perform reliable operations between standing qubits and arbitrarily shaped traveling photons. The method was used to generate fast (2.5 μs) remote entanglement of two qubits separated by $\sim$1 m microwave cables and a circulator. This protocol could be readily extended to entangle larger systems in order to detect photon loss in the transmission line [14,33,34]. Moreover, by controlling

the traveling photon wave packet shape in frequency, the signal from one cavity could be routed to another arbitrary one connected on the same line. All these features are important primitives on the path to a reliable modular quantum computing architecture [13] or quantum internet [11].

The authors thank Z. Leghtas, A. Grimm, and S. Touzard for helpful discussions, and M. Rooks for fabrication assistance. Facilities use was supported by the Yale Institute for Nanoscience and Quantum Engineering (YINQE), the National Science Foundation (NSF) MRSEC DMR 1119826, and the Yale School of Engineering and Applied Sciences clean room. This research was supported by the U.S. Army Research Office (Grants No. W911NF-14-1-0011 and No. AWD0001152), and the Multidisciplinary University Research Initiative through the U.S. Air Force Office of Scientific Research (Grant No. FP057123-C). L. B. acknowledges support of the ARO QuaCGR Fellowship. P. R. is also supported by the U.S. Air Force Office of Scientific Research, Grant No. FA9550-15-1-0015.

*philippe.campagne-ibarcq@yale.edu
†michel.devoret@yale.edu

[1] E. Schrödinger, Discussion of probability relations between separated systems, in *Mathematical Proceedings of the Cambridge Philosophical Society*, Vol. 31 (Cambridge University Press, Cambridge, England, 1935), pp. 555–563.
[2] R. Jozsa and N. Linden, On the role of entanglement in quantum-computational speed-up, in *Proceedings of the Royal Society of London A: Mathematical, Physical and Engineering Sciences*, Vol. 459 (The Royal Society, London, 2003), pp. 2011–2032.
[3] J. Hofmann, M. Krug, N. Ortegel, L. Gérard, M. Weber, W. Rosenfeld, and H. Weinfurter, Heralded entanglement between widely separated atoms, Science **337**, 72 (2012).
[4] B. Julsgaard, A. Kozhekin, and E. S. Polzik, Experimental long-lived entanglement of two macroscopic objects, Nature (London) **413**, 400 (2001).
[5] N. Roch, M. E. Schwartz, F. Motzoi, C. Macklin, R. Vijay, A. W. Eddins, A. N. Korotkov, K. B. Whaley, M. Sarovar, and I. Siddiqi, Observation of Measurement-Induced Entanglement and Quantum Trajectories of Remote Superconducting Qubits, Phys. Rev. Lett. **112**, 170501 (2014).
[6] C. Dickel, J. J. Wesdorp, N. K. Langford, S. Peiter, R. Sagastizabal, A. Bruno, B. Criger, F. Motzoi, and L. DiCarlo, Chip-to-chip entanglement of transmon qubits using engineered measurement fields, Phys. Rev. B **97**, 064508 (2018).
[7] D. L. Moehring, P. Maunz, S. Olmschenk, K. C. Younge, D. N. Matsukevich, L.-M. Duan, and C. Monroe, Entanglement of single-atom quantum bits at a distance, Nature (London) **449**, 68 (2007).
[8] H. Bernien, B. Hensen, W. Pfaff, G. Koolstra, M. S. Blok, L. Robledo, T. H. Taminiau, M. Markham, D. J. Twitchen, L. Childress *et al.*, Heralded entanglement between solid-state qubits separated by three metres, Nature (London) **497**, 86 (2013).
[9] A. Delteil, Z. Sun, W.-b. Gao, E. Togan, S. Faelt, and A. Imamoglu, Generation of heralded entanglement between distant hole spins, Nat. Phys. **12**, 218 (2016).
[10] A. Narla, S. Shankar, M. Hatridge, Z. Leghtas, K. M. Sliwa, E. Zalys-Geller, S. O. Mundhada, W. Pfaff, L. Frunzio, R. J. Schoelkopf *et al.*, Robust Concurrent Remote Entanglement between Two Superconducting Qubits, Phys. Rev. X **6**, 031036 (2016).
[11] H. J. Kimble, The quantum internet, Nature (London) **453**, 1023 (2008).
[12] L.-M. Duan and C. Monroe, Colloquium: Quantum networks with trapped ions, Rev. Mod. Phys. **82**, 1209 (2010).
[13] C. Monroe, R. Raussendorf, A. Ruthven, K. R. Brown, P. Maunz, L.-M. Duan, and J. Kim, Large-scale modular quantum-computer architecture with atomic memory and photonic interconnects, Phys. Rev. A **89**, 022317 (2014).
[14] D. N. Matsukevich, T. Chaneliere, S. D. Jenkins, S.-Y. Lan, T. A. B. Kennedy, and A. Kuzmich, Entanglement of Remote Atomic Qubits, Phys. Rev. Lett. **96**, 030405 (2006).
[15] J. I. Cirac, P. Zoller, H. J. Kimble, and H. Mabuchi, Quantum State Transfer and Entanglement Distribution among Distant Nodes in a Quantum Network, Phys. Rev. Lett. **78**, 3221 (1997).
[16] M. Keller, B. Lange, K. Hayasaka, W. Lange, and H. Walther, Continuous generation of single photons with controlled waveform in an ion-trap cavity system, Nature (London) **431**, 1075 (2004).
[17] A. A. Houck, D. I. Schuster, J. M. Gambetta, J. A. Schreier, B. R. Johnson, J. M. Chow, L. Frunzio, J. Majer, M. H. Devoret, S. M. Girvin *et al.*, Generating single microwave photons in a circuit, Nature (London) **449**, 328 (2007).
[18] S. J. Srinivasan, N. M. Sundaresan, D. Sadri, Y. Liu, J. M. Gambetta, T. Yu, S. M. Girvin, and A. A. Houck, Time-reversal symmetrization of spontaneous emission for quantum state transfer, Phys. Rev. A **89**, 033857 (2014).
[19] M. Pechal, L. Huthmacher, C. Eichler, S. Zeytinoğlu, A. A. Abdumalikov, Jr., S. Berger, A. Wallraff, and S. Filipp, Microwave-Controlled Generation of Shaped Single Photons in Circuit Quantum Electrodynamics, Phys. Rev. X **4**, 041010 (2014).
[20] W. F. Kindel, M. D. Schroer, and K. W. Lehnert, Generation and efficient measurement of single photons from fixed-frequency superconducting qubits, Phys. Rev. A **93**, 033817 (2016).
[21] W. Pfaff, C. J. Axline, L. D. Burkhart, U. Vool, P. Reinhold, L. Frunzio, L. Jiang, M. H. Devoret, and R. J. Schoelkopf, Controlled release of multiphoton quantum states from a microwave cavity memory, Nat. Phys. **13**, 882 (2017).
[22] T. A. Palomaki, J. W. Harlow, J. D. Teufel, R. W. Simmonds, and K. W. Lehnert, Coherent state transfer between itinerant microwave fields and a mechanical oscillator, Nature (London) **495**, 210 (2013).
[23] J. Wenner, Y. Yin, Y. Chen, R. Barends, B. Chiaro, E. Jeffrey, J. Kelly, A. Megrant, J. Y. Mutus, C. Neill *et al.*, Catching Time-Reversed Microwave Coherent State Photons with 99.4% Absorption Efficiency, Phys. Rev. Lett. **112**, 210501 (2014).

[24] M. Pierre, I.-M. Svensson, S. R. Sathyamoorthy, G. Johansson, and P. Delsing, Storage and on-demand release of microwaves using superconducting resonators with tunable coupling, Appl. Phys. Lett. **104**, 232604 (2014).

[25] E. Flurin, N. Roch, J.-D. Pillet, F. Mallet, and B. Huard, Superconducting Quantum Node for Entanglement and Storage of Microwave Radiation, Phys. Rev. Lett. **114**, 090503 (2015).

[26] A. N. Korotkov, Flying microwave qubits with nearly perfect transfer efficiency, Phys. Rev. B **84**, 014510 (2011).

[27] Y. Yin, Y. Chen, D. Sank, P. J. J. O'Malley, T. C. White, R. Barends, J. Kelly, E. Lucero, M. Mariantoni, A. Megrant *et al.*, Catch and Release of Microwave Photon States, Phys. Rev. Lett. **110**, 107001 (2013).

[28] R. W. Andrews, A. P. Reed, K. Cicak, J. D. Teufel, and K. W. Lehnert, Quantum-enabled temporal and spectral mode conversion of microwave signals, Nat. Commun. **6**, 10021 (2015).

[29] K. Inomata, Z. Lin, K. Koshino, W. D. Oliver, J.-S. Tsai, T. Yamamoto, and Y. Nakamura, Single microwave-photon detector using an artificial Λ-type three-level system, Nat. Commun. **7**, 12303 (2016).

[30] Recently, similar results were reported by two other groups [31,32].

[31] C. Axline, L. Burkhart, W. Pfaff, M. Zhang, K. Chou, P. Campagne-Ibarcq, P. Reinhold, L. Frunzio, S. M. Girvin, L. Jiang *et al.*, On-demand quantum state transfer and entanglement between remote microwave cavity memories, arXiv:1712.05832.

[32] P. Kurpiers, P. Magnard, T. Walter, B. Royer, M. Pechal, J. Heinsoo, Y. Salathé, A. Akin, S. Storz, J.-C. Besse *et al.*, Deterministic quantum state transfer and generation of remote entanglement using microwave photons, arXiv: 1712.08593.

[33] C. H. Bennett, G. Brassard, S. Popescu, B. Schumacher, J. A. Smolin, and W. K. Wootters, Purification of Noisy Entanglement and Faithful Teleportation via Noisy Channels, Phys. Rev. Lett. **76**, 722 (1996).

[34] N. Kalb, A. A. Reiserer, P. C. Humphreys, J. J. W. Bakermans, S. J. Kamerling, N. H. Nickerson, S. C. Benjamin, D. J. Twitchen, M. Markham, and R. Hanson, Entanglement distillation between solid-state quantum network nodes, Science **356**, 928 (2017).

[35] H. Paik, D. I. Schuster, L. S. Bishop, G. Kirchmair, G. Catelani, A. P. Sears, B. R. Johnson, M. J. Reagor, L. Frunzio, L. I. Glazman *et al.*, Observation of High Coherence in Josephson Junction Qubits Measured in a Three-Dimensional Circuit QED Architecture, Phys. Rev. Lett. **107**, 240501 (2011).

[36] See Supplemental Material at http://link.aps.org/supplemental/10.1103/PhysRevLett.120.200501 for system characterization, details of the experimental setup, and control pulses generation algorithm, which includes Refs. [37–39].

[37] K. Geerlings, Z. Leghtas, I. M. Pop, S. Shankar, L. Frunzio, R. J. Schoelkopf, M. Mirrahimi, and M. H. Devoret, Demonstrating a Driven Reset Protocol for a Superconducting Qubit, Phys. Rev. Lett. **110**, 120501 (2013).

[38] J. Gambetta, A. Blais, M. Boissonneault, A. A. Houck, D. I. Schuster, and S. M. Girvin, Quantum trajectory approach to circuit QED: Quantum jumps and the Zeno effect, Phys. Rev. A **77**, 012112 (2008).

[39] S. E. Nigg, H. Paik, B. Vlastakis, G. Kirchmair, S. Shankar, L. Frunzio, M. H. Devoret, R. J. Schoelkopf, and S. M. Girvin, Black-Box Superconducting Circuit Quantization, Phys. Rev. Lett. **108**, 240502 (2012).

[40] A. Wallraff, D. I. Schuster, A. Blais, J. M. Gambetta, J. Schreier, L. Frunzio, M. H. Devoret, S. M. Girvin, and R. J. Schoelkopf, Sideband Transitions and Two-Tone Spectroscopy of a Superconducting Qubit Strongly Coupled to an On-Chip Cavity, Phys. Rev. Lett. **99**, 050501 (2007).

[41] M. Mirrahimi, Z. Leghtas, V. V. Albert, S. Touzard, R. J. Schoelkopf, L. Jiang, and M. H. Devoret, Dynamically protected cat-qubits: A new paradigm for universal quantum computation, New J. Phys. **16**, 045014 (2014).

[42] Z. Leghtas, S. Touzard, I. M. Pop, A. Kou, B. Vlastakis, A. Petrenko, K. M. Sliwa, A. Narla, S. Shankar, M. J. Hatridge *et al.*, Confining the state of light to a quantum manifold by engineered two-photon loss, Science **347**, 853 (2015).

[43] A. Blais, R.-S. Huang, A. Wallraff, S. M. Girvin, and R. Jun Schoelkopf, Cavity quantum electrodynamics for superconducting electrical circuits: An architecture for quantum computation, Phys. Rev. A **69**, 062320 (2004).

[44] N. Bergeal, F. Schackert, M. Metcalfe, R. Vijay, V. E. Manucharyan, L. Frunzio, D. E. Prober, R. J. Schoelkopf, S. M. Girvin, and M. H. Devoret, Phase-preserving amplification near the quantum limit with a Josephson ring modulator, Nature (London) **465**, 64 (2010).

[45] N. Roch, E. Flurin, F. Nguyen, P. Morfin, P. Campagne-Ibarcq, M. H. Devoret, and B. Huard, Widely Tunable, Nondegenerate Three-Wave Mixing Microwave Device Operating Near the Quantum Limit, Phys. Rev. Lett. **108**, 147701 (2012).

[46] D. Riste, J. G. Van Leeuwen, H.-S. Ku, K. W. Lehnert, and L. DiCarlo, Initialization by Measurement of a Superconducting Quantum Bit Circuit, Phys. Rev. Lett. **109**, 050507 (2012).

[47] P. Campagne-Ibarcq, E. Flurin, N. Roch, D. Darson, P. Morfin, M. Mirrahimi, M. H. Devoret, F. Mallet, and B. Huard, Persistent Control of a Superconducting Qubit by Stroboscopic Measurement Feedback, Phys. Rev. X **3**, 021008 (2013).

[48] C. Gardiner and P. Zoller, *Quantum Noise: A Handbook of Markovian and Non-Markovian Quantum Stochastic Methods with Applications to Quantum Optics*, Vol. 56 (Springer-Verlag, Berlin, Heidelberg, 2004).

[49] P. Magnard, P. Kurpiers, B. Royer, T. Walter, J.-C. Besse, S. Gasparinetti, M. Pechal, J. Heinsoo, S. Storz, A. Blais *et al.*, Fast and unconditional all-microwave reset of a superconducting qubit, arXiv:1801.07689.

[50] J.-C. Besse, S. Gasparinetti, M. C. Collodo, T. Walter, P. Kurpiers, M. Pechal, C. Eichler, and A. Wallraff, Single-Shot Quantum Nondemolition Detection of Individual Itinerant Microwave Photons, Phys. Rev. X **8**, 021003 (2018).

[51] S. Kono, K. Koshino, Y. Tabuchi, A. Noguchi, and Y. Nakamura, Quantum non-demolition detection of an itinerant microwave photon, arXiv:1711.05479.